THz Letters

A Linear-Array of 300-GHz Antenna Integrated GFET Detectors on a Flexible Substrate

Xinxin Yang , *Student Member, IEEE*, Andrei Vorobiev , *Member, IEEE*, Jian Yang , *Member, IEEE*, Kjell Jeppson , *Life Member, IEEE*, and Jan Stake , *Senior Member, IEEE*

Abstract—Terahertz imaging has potential in a variety of applications, such as noninvasive inspection, medical examination, and security. Many of these applications call for flexible focal-plane arrays with large fields of view. Here, we demonstrate the implementation of a flexible, 300 GHz, 1×6 linear detector array based on graphene field-effect transistors and integrated bow-tie antennas. Conservative estimates based on room temperature measurements at 300 GHz show element voltage responsivities in the range from 20 to 70 V/W, and noise equivalent powers in the range from 0.06 to 0.2 nW/$\sqrt{\text{Hz}}$. Measured radiation patterns, showing good agreement with simulations, reveal half-power beamwidths of $45°$ and $60°$ for *H*- and *E*-planes, respectively. Characterization of the antenna array in a curved configuration shows that the voltage response is reduced up to 3 dB compared to the flat configuration due to a decrease of the antenna directivity. We believe that our preliminary results could serve as an enabling platform for the future development of flexible antenna arrays based on graphene field-effect transistors for curved focal plane imaging, important for wearable sensors and many other applications.

Index Terms—Antenna arrays, field-effect transistors, flexible electronics, graphene, terahertz detectors, two-dimensional (2-D) materials, radiation patterns.

I. INTRODUCTION

TERAHERTZ (THz) imaging is a promising technique for many applications [1]. With the development of high-speed terahertz detectors, flat focal-plane arrays for terahertz imaging have been successfully implemented in different technologies, using detectors based on complementary metal oxide semiconductor transistors [2], [3], high electron mobility transistors [4],

Schottky barrier diodes [5], and heterojunction backward diodes [6]. Curved arrays, with advantages such as larger field of view, better image quality, shape-conforming integration, and simplification of the optical systems, have been demonstrated in the frequency range of visible and near-infrared light [7]–[9]. In 2016, Suzuki *et al*. demonstrated the first flexible detector array based on carbon nanotubes [10] for terahertz imaging. However, the low sensitivity of carbon nanotube detectors limits the possibilities of this technology.

In recent years, the rise of graphene with its high carrier mobility and flexibility has provided new inspiration for the development of terahertz imaging and sensing. Detectors based on graphene field-effect transistors (GFETs) have shown their potential for wide-band, high-speed, and high-sensitivity terahertz detection [11]–[13]. Moreover, our previous study has shown that GFETs can be used for flexible terahertz detection [14].

In this letter, we present the demonstration of a 1×6 linear array based on GFETs coupled with 300-GHz bow-tie antennas on a flexible substrate in both flat and curved configurations. In addition, the radiation patterns of one pixel are measured and compared to simulated results.

II. DESIGN, FABRICATION AND EXPERIMENTAL METHODS

This section describes the design and fabrication of the flexible GFET detector array, and the measurement setup for array characterization. Each array consists of six GFET detectors with integrated bow–tie antennas as shown in Fig. 1. For symmetry reasons, dummy antennas were placed at either end of the array in order to keep the radiation pattern for each pixel equal. Each pixel element of the array is formed as a two-terminal detector, where the incoming RF-signal is coupled to both the gate and the drain terminals. All detectors in the array are connected to a common source and designed using a quasi-static model based on the nonlinear dc-characteristics [15]. Based on previous experience the GFET gate length of 1.4 μm and a gate width of 6.8 μm was chosen for obtaining a small-signal device impedance of 70 Ω at 300 GHz. The design of the bow–tie antenna array was optimized using the CST studio suite finite-difference-time-domain electromagnetic solver. As a result, an antenna radius of 180 μm was selected to optimize
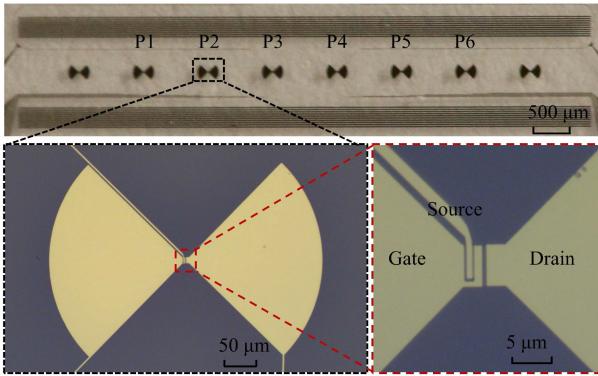
Fig. 1. Detector array. Photograph of the linear-array and optical microscopy images of a single pixel element.
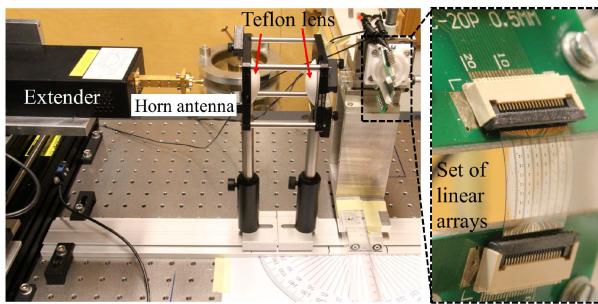

Fig. 2. Experimental setup. Photographs of the experimental setup for terahertz characterization and the set of linear arrays under test for curved configuration with radius of curvature 13 mm.

the gain at 300 GHz. The center-to-center pixel distance was set to 900 μm considering the diffraction limit of a terahertz wave at 300 GHz. Two parallel metal strip arrays were placed, one on each side of the GFET detector array, in order to increase the H-plane directivity.

A set of linear arrays were fabricated using monolayer chemical vapor deposition (CVD) graphene provided by Graphenea on polyethylene naphthalate substrates (125 μm thick). To reduce contaminations during following processing steps, the graphene was first covered with a Al_2O_3 layer by repeating four times a sequence of depositing 1 nm Al layers and natural oxidizing. After the areas for the graphene mesa were defined by e-beam lithography, the Al_2O_3 and the graphene outside the mesa were removed by buffered oxide etch and oxygen plasma, respectively. Then, the source and drain electrodes were patterned by a sequence of e-beam lithography, Al_2O_3 etch, Ti/Pd/Au (1 nm/15 nm/250 nm) deposition, and lift-off. After patterning of the gate area by e-beam lithography, the gate dielectric was deposited by repeating six times a sequence of depositing 1 nm Al layers and natural oxidizing. Finally, the gate electrodes and the parallel metal strip array were formed by using Al/Au (150 nm/ 100 nm) deposition and lift-off technology.

The detector array was characterized using the experimental setup shown in Fig. 2. The 300-GHz signal was provided by an Agilent HP 83650A signal generator and a VDI WR-3.4 extender mounted on a motorized x–y translation stage. The

terahertz signal was transmitted by a horn antenna mounted on the waveguide flange of the extender and focused onto the detector array through two polytetrafluoroethylene (PTFE) Teflon lenses. The array sample under test was mounted between, and electrically connected to, two printed circuit boards (PCBs). Each PCB was attached to a PTFE Teflon beam mounted in a circular trench of a specially designed and fabricated PTFE Teflon fixture mounted on a three-axis translation stage. By moving the two beams along the circular trench, the PCBs could be tilted, thereby bending the detector array into a circular arc in vertical plane. The linear scan was made by moving the extender vertically.

During characterization, the GFET detectors were operated without drain bias to minimize $1/f$ noise, and the gate bias (V_{GS}) was provided by a Keithley 2604B source meter. The rectified detector voltage signal, ΔU, between the drain and the source was measured using an SR830 lock-in amplifier with a modulation frequency of 777 Hz. The available output signal power, P_{ava}, was measured at the waveguide flange of the extender using a VDI Erickson PM5 power meter with a taper waveguide section.

III. RESULTS AND DISCUSSION

First, dc characterization was performed to obtain the GFET resistance R_{DS} versus gate voltage V_{GS} characteristics at a low drain voltage (10 mV). The detectors were then characterized at 300 GHz for obtaining the voltage responsivity $\Re_V$, and the equivalent noise power (NEP). The voltage responsivity of the detectors was obtained from [14],

$$\Re_V = \frac{2\sqrt{2}\Delta U}{P_{ava}} \qquad (1)$$

where the factor $2\sqrt{2}$ is for compensating the peak-to-peak amplitude of the input signal, and for the lock-in amplifier displaying the measured signal in volts rms. Still, we believe that the voltage responsivity is underestimated since possible power losses in the experimental setup are neglected, and since not all of the input signal may be received by the antenna. Fig. 3 (a) shows the voltage responsivity of the six pixels (numbered P1 to P6) of a 1×6-pixel detector array as a function of the gate voltage overdrive from the Dirac point voltage ($V_{GS} - V_{Dir}$). Overall, the individual pixel detectors of the array show similar behavior, but with certain variations in amplitude. For all detectors, the voltage responsivity goes to zero close to the Dirac point voltage. The values observed for the peak voltage responsivity are in the range from 20 to 70 V/W for gate voltage overdrives at, or close to, 1 V.

For calculating the noise equivalent power, the GFET detector is considered having a resistance $R_{DS} = V_{DS}/I_{DS}$ obtained from the dc characterization mentioned above. Assuming a thermal noise power spectral density of $4k_BTR_{DS}$, k_B is the Boltzmann's constant, T is the temperature, the NEP for the six pixels from Fig. 3(a) can obtained as shown in Fig. 3(b) [14]. The minimum NEP observed is in the range from 0.06 to 0.2 nW/$\sqrt{Hz}$. The pixel-to-pixel variations of the voltage responsivity and the NEP can be associated with both inherent
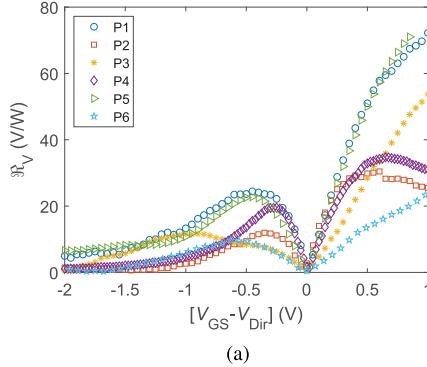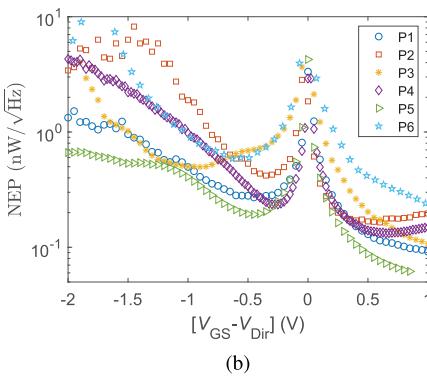
Fig. 3.   Responsivity and noise equivalent power. 300-GHz voltage responsivity (a) and noise equivalent power (b) of the six pixels of the detector array in flat configuration with incident beam normal to each pixel as a function of $V_{\mathrm{GS}} - V_{\mathrm{Dir}}$ without drain bias.
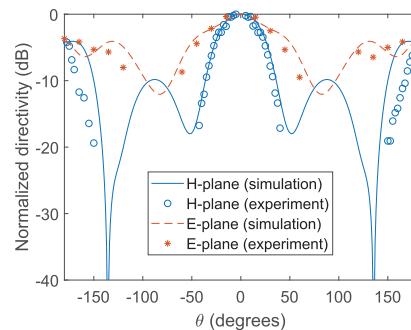

Fig. 4.   Measured (symbols) and simulated (lines) H- and E-plane radiation patterns of one pixel in flat configuration.

nonuniformities of CVD graphene grown on copper substrates, and to the still somewhat immature technology used for fabrication of GFETs and its interfaces.

Fig. 4 shows the measured and simulated radiation patterns of one detector pixel at 300 GHz. The measured radiation pattern are determined by the rectified output voltage of the pixel rotating over its H- and E-planes. The half power beam widths of the antenna are $45°$ and $60°$ for H- and E-planes, respectively, which is in good agreement with simulation results.

Fig. 5(a) and (b) show the measured voltage response of the six pixels of the detector array in flat configuration and in a curved configuration with a radius of 13 mm, respectively, normalized
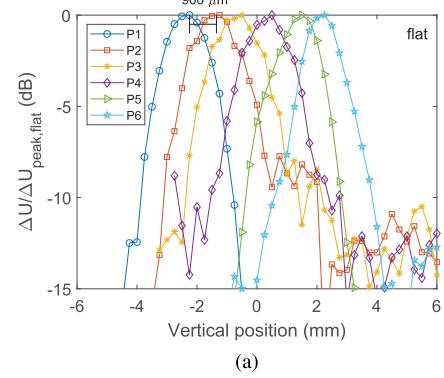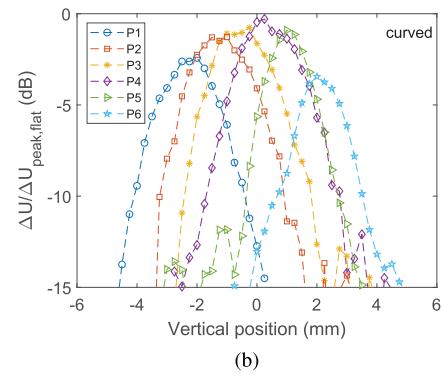

Fig. 5.   Measurements showing the detector voltage responses for the six pixels of an array normalized to their peak values versus the vertical position of the transmitter in the incidence plane in flat (a) and curved (b) configurations.

TABLE I
COMPARISON OF ROOM-TEMPERATURE TERAHERTZ DETECTORS
BASED ON ANTENNA-INTEGRATED GFETs

Ref.	$\Re_V$ (V/W)	NEP (nW/$\sqrt{\mathrm{Hz}}$)	Frequency (GHz)	Substrate
This work	20-70	0.06-0.2	300	PEN
Yang, et al.[14]	2	3	487	PET
Qin, et al.[13]	30	0.05	330	SiC
Generalov, et al.[12]	74	0.1	400	Si/SiO$_2$
Zak, et al.[16]	14	0.5	600	Si/SiO$_2$
Vicarelli, et al. [11]	0.15	30	300	Si/SiO$_2$

to the peak value as a function of the vertical position of the extender. The peak value of the voltage response in the curved configuration is found to be from 0.1 to 3 dB less than that in the flat configuration. These differences are due to a decrease of the directive gain for pixel detectors in the curved configuration, since their boresight axes are no longer in line with the incoming wave, see Fig. 4.

IV. CONCLUSION

A flexible 300 GHz 1×6 linear antenna array based on GFET detectors with integrated bow–tie antennas has been demonstrated. A conservative approach shows voltage

responsivity estimates in the range from 20 to 70 V/W, and a noise equivalent power in the range from 0.06 to 0.2 nW/$\sqrt{Hz}$ for pixel detectors in flat configuration. A comparison of the terahertz voltage responsivity and NEP for antenna integrated-GFETs on different substrates is shown in Table I. Measurements show that the half-power beam widths of the antenna radiation pattern are $45°$ and $60°$ for the H- and E-planes, respectively, which agrees well with simulation results. Measurements also show that the voltage response for pixels in curved configuration is reduced up to 3 dB due to a decrease of antenna directivity. Although the detector array is still limited in size, we believe that large flexible arrays, both with linear and 2-D focal planes, will become a reality as GFET fabrication processes improve and inherent nonuniformities could be controlled. This development would allow us to bring many exciting terahertz applications into reality.

REFERENCES

[1] P. Hillger, J. Grzyb, R. Jain, and U. R. Pfeiffer, "Terahertz imaging and sensing applications with silicon-based technologies," *IEEE Trans. Terahertz Sci. Technol.*, vol. 9, no. 1, pp. 1–19, Jan. 2019.

[2] S. Boppel, A. Lisauskas, A. Max, V. Krozer, and H. G. Roskos, "CMOS detector arrays in a virtual 10-kilopixel camera for coherent terahertz real-time imaging," *Opt. Lett.*, vol. 37, no. 4, pp. 536–538, 2012, doi: 10.1364/OL.37.000536.

[3] H. Sherry *et al.*, "A 1kPixel CMOS camera chip for 25fps real-time terahertz imaging applications," in *IEEE Int. Solid-State Circuits Conf.*, 2012, pp. 252–254, doi: 10.1109/ISSCC.2012.6176997.

[4] M. Li *et al.*, "340 GHz lens-coupled 4×4 GaAs detector array for terahertz imaging applications," *Elect. Letters*, vol. 54, no. 20, pp. 1180–1182, 2018, doi: 10.1049/el.2018.5856.

[5] R. Han *et al.*, "Active terahertz imaging using Schottky diodes in CMOS: Array and 860-GHz pixel," *IEEE J. Solid-State Circuits*, vol. 48, no. 10, pp. 2296–2308, Oct. 2013.

[6] G. C. Trichopoulos, H. L. Mosbacker, D. Burdette, and K. Sertel, "A broadband focal plane array camera for real-time THz imaging applications," *IEEE Trans. Antennas. Propag.*, vol. 61, no. 4, pp. 1733–1740, Apr. 2013.

[7] H. C. Ko *et al.*, "A hemispherical electronic eye camera based on compressible silicon optoelectronics," *Nature*, vol. 454, no. 7205, pp. 748–753, 2008, doi: 10.1038/nature07113.

[8] S.-B. Rim, P. B. Catrysse, R. Dinyari, K. Huang, and P. Peumans, "The optical advantages of curved focal plane arrays," *Opt. Express*, vol. 16, no. 7, pp. 4965–4971, 2008, doi: 10.1364/OE.16.004965.

[9] M. Fendler *et al.*, "Hemispherical infrared focal plane arrays: A new design parameter for the instruments," in *High Energy, Optical, and Infrared Detectors for Astronomy V*, vol. 8453. Int. Soc. Optics Photon., 2012, paper 84531, doi: 10.1117/12.925379.

[10] D. Suzuki, S. Oda, and Y. Kawano, "A flexible and wearable terahertz scanner," *Nat. Photon.*, vol. 10, no. 12, pp. 809–813, 2016, doi: 10.1038/NPHOTON.2016.209.

[11] L. Vicarelli *et al.*, "Graphene field-effect transistors as room-temperature terahertz detectors," *Nat. Mater.*, vol. 11, no. 10, pp. 865–871, 2012, doi: 10.1038/nmat3417.

[12] A. A. Generalov, M. A. Andersson, X. Yang, A. Vorobiev, and J. Stake, "A 400-GHz graphene fet detector," *IEEE Trans. Terahertz Sci. Technol.*, vol. 7, no. 5, pp. 614–616, Sep. 2017.

[13] H. Qin *et al.*, "Room-temperature, low-impedance and high-sensitivity terahertz direct detector based on bilayer graphene field-effect transistor," *Carbon*, vol. 116, pp. 760–765, 2017, doi: 10.1016/j.carbon.2017.02.037.

[14] X. Yang, A. Vorobiev, A. Generalov, M. A. Andersson, and J. Stake, "A flexible graphene terahertz detector," *Appl. Phys. Lett.*, vol. 111, no. 2, 2017, Art. no. 021102, doi: 10.1063/1.4993434.

[15] X. Yang, A. Vorobiev, K. Jeppson, and J. Stake, "Describing broadband terahertz response of graphene FET detectors by a classical model," *IEEE Trans. Terahertz Sci. Technol*, vol. 10, no. 2, pp. 158–166, Mar. 2020.

[16] A. Zak *et al.*, "Antenna-integrated 0.6 THz FET direct detectors based on CVD graphene," *Nano Lett.*, vol. 14, no. 10, pp. 5834–5838, 2014, doi: 10.1021/nl5027309.